Elastic properties and indentation cracking behavior of Na2O-TiO2-SiO2 glasses

Garth Scannell, Liping Huang, Tanguy Rouxel

Elastic properties and indentation cracking behavior of Na_2O-TiO_2-SiO_2 glasses

Garth Scannell[1,2], Liping Huang[1,*] and Tanguy Rouxel[2,*]

[1]Department of Materials Science and Engineering, Rensselaer Polytechnic Institute, Troy, NY 12180, USA
[2]Glass and Mechanics Department, Université of Rennes 1, Rennes, 35042 RENNES CEDEX, France

Abstract
The effects of composition on indentation deformation and cracking behavior of Na_2O-TiO_2-SiO_2 glasses were studied in the light of structural considerations and parameters such as the atomic packing density (C_g) and the network energy, using a combination of elastic measurements and micro-hardness indentation experiments. Na_2O-TiO_2-SiO_2 glasses with titania contents of 4-10 mol% and sodium oxide contents of 10-25 mol% were prepared through a traditional melt-quench process. Indentation experiments were conducted using a Vickers indenter with loads ranging from 10 mN to 49 N. Critical loads for crack initiation and cracking patterns were systematically investigated and correlated with the elastic properties of glass. In this ternary system concerning a relatively large range of Poisson's ratio (ν), a minimum in critical crack initiation load was observed at a ν of 0.21-0.22. This study brings to light the unusual role of titanium in the glass network, that give birth to peculiar trends in the structural and mechanical properties.

Keywords: Sodium-titanium-silicate glass; Young's modulus; Vickers hardness; Crack initiation load; Poisson's ratio

---

[*] Corresponding authors. E-mail address: huangL5@rpi.edu (L. Huang), tanguy.rouxel@univ-rennes1.fr (T. Rouxel)

1. Introduction

An intriguing correlation was observed recently in oxide glasses and in metallic glasses: the fracture energy (G) increases with the Poisson's ratio (v), with a sharp brittle-to-ductile (BTD) transition at a critical v_{BTD}=0.31-0.32 [1]. A similar Poisson's ratio-ductility correlation has also been reported in crystalline metals [2]. Recently, Rouxel also showed that densified silica, when v increases from 0.15 to 0.25, is capable of shear flow under indentation resulting in pile-ups [3] and found that v is directly correlated with the atomic packing density (C_g) and the glass network dimensionality [4]. Such a far-from-equilibrium fracture property versus near-equilibrium elastic property relation is quite unexpected, yet highly beneficial by setting v as an optimization target to make stronger and tougher glasses. The precise measurement of fracture toughness and the associated fracture energy requires large samples and tedious sample preparation. However, elastic characteristics, especially Poisson's ratio can be measured relatively easily, using much smaller samples, such as mm sized samples for ultrasonic measurements and tens of μm sized samples for Brillouin light scattering experiments. In both methods, v can be easily calculated from the measured longitudinal $_{(V_L)}$ and transverse $_{(V_T)}$ sound velocities: $v = (V_L^2 - 2V_T^2)/[2(V_L^2 - V_T^2)]$. The v-G relation has already been proposed as a guide to obtain tough metallic glasses [5,6]. It is of great scientific and technological interest to investigate whether a similar relation holds in oxide glasses, as stronger and tougher glasses are increasingly demanded for applications such as personal electronics, windows for transportation systems, architectural materials, solar panels, and submarine communications cables, etc.

Indentation is a relatively simple way to observe the mechanical behavior of glass and the initiation of cracks under contact loading. Wada et al. described the susceptibility to cracking in a glass by its crack resistance, or the critical load to initiate two cracks from a Vickers indentation [7]. Sehgal and Ito [8] used a "brittleness" index, proposed by Lawn and Marshall as a ratio of hardness to fracture toughness [9], as a measure of glass resistance toward cracking. However, it is unclear whether this relationship is sufficiently refined to allow for the comparison of glasses with slight changes in composition. Additionally, Kato et al. showed that the crack resistance does not have a clear relationship with either Vickers hardness or the fracture toughness [10]. It seems that to predict the cracking behavior of glass under indentation, the effects of permanent deformation during indentation (densification and shear flow) on the stress field need to be better understood. At lower v, the primary mode of deformation under indentation is densification, as v increases, a shift from densification to shear flow is expected [3]. This shift is accompanied by a change in the cracking behavior [11].

In this work, we examine whether relationships between the mechanical properties measured through indentation and the v exist by focusing on soda-titania-silicate glasses covering a range of v from 0.18 to 0.24. The Na$_2$O-TiO$_2$-SiO$_2$ glass system was chosen because it covered a large range of Poisson's ratio, both Na$_2$O and TiO$_2$ are known to separately cause unusual behavior in silicate glasses (anomalous elastic moduli behavior with respect to temperature and anomalous thermal expansion respectively).

To understand the elastic properties and the indentation behaviors of glass, it is important to consider the glasses from a structural standpoint. The basic bonding environment of Si and Na is fairly well known, with Si forming tetrahedrally coordinated with four oxygen atoms and Na breaking a Si-O-Si bond to form a nonbridging oxygen, Si-O-Na. The basic bonding environment of Ti is more complicated, being able to adopt four, five, or six-fold coordinations, depending on the concentration and species of the other cations present in the glass. Farges, et

al. found that in Na_2O-TiO_2-SiO_2 glasses, Ti primarily adopts a fivefold coordination with a square pyramidal geometry, with four bridging oxygens and one double bonded nonbridging oxygen [12,13]. The effect of TiO_2 on the mechanical properties and the structure of glasses depends strongly on its coordination state, and is still poorly understood.

2 Experimental details

Soda-titania-silicate glasses were synthesized through a traditional melt-quench method from powders. Glasses with compositions of $(x)Na_2O$-$(y)TiO_2$-$(1-x-y)SiO_2$, where x=10, 15, 20, and 25 and y=4, 7, and 10 mol%, were chosen to cover a range of Poisson's ratios (v=0.18-0.24). Powders used were of 99% purity or higher. Powders were mixed for approximately 30 minutes and then melted in a Pt or a 10%Rh-90%Pt crucible at 1400-1500 °C for three hours, with the powder added in three to four intervals during the first hour. The temperature was increased to 1600-1700 °C for ten minutes prior to quenching to make pouring the glass easier. After pouring, the glasses were quickly transferred into an annealing furnace set slightly above their glass transition temperatures (550-600 °C) for 1-2 hours and furnace cooled overnight. Glasses were visually checked for residual stresses using a polarizer and re-melted if excessive residual stresses were observed.

For indentation experiments, samples of approximately 10 mm x 10 mm x 4 mm were prepared. Samples were cut using a diamond saw and two parallel faces were polished with 240, 400, and 600 grit Al_2O_3 paper followed by a cerium oxide slurry.

Vickers indents were made using a Matsuzawa hardness indenter at 49 N, 9.8 N, 4.9 N, and 2.9 N and using a Fischer indenter at 1 N, 0.5 N, and 0.1 N. Ten indents were made at each load and images of each indent were taken using either an Olympus BX60 optical microscope or a scanning electron microscope (SEM) for indents made with the Matsuzawa and the Fischer indention machine, respectively. Apparent surface roughness/scratches in some of the images is due to residual organics from temporary storage in soft plastic containers, which was removed with alcohol/acetone after the problem was observed in initial samples. All indentations were done in air, cracking patterns surrounding indents were studied after crack growth had stopped. To determine when crack growth had stopped, images of indents across four compositions (x=10, 15, 20, 25 and y=4) were taken at 5 images/sec for up to 24 hours. Crack growth stopped and no new cracks appeared after two hours for all compositions. Fig. 1 shows the crack growth around a 1 kg indent in a $15Na_2O$-$4TiO_2$-$81SiO_2$ glass over a 20 hour period. In order to compare the behavior of glasses with different compositions regardless of environmental fatigue effects, it was decided to investigate the indentation patterns at least two hours after indentation.
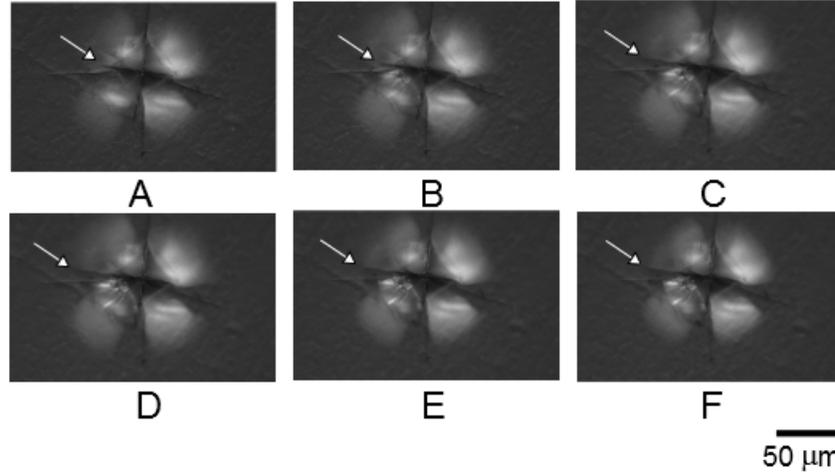
Fig. 1. Optical microscope images showing crack growth around a 1 kg Vickers indent in a $15Na_2O$-$4TiO_2$-$81SiO_2$ glass at 5 minutes (A), 30 minutes (B), 1 hour (C), 2 hours (D), 10 hours (E), and 20 hours (F). Crack growth is significant over the first hour, slight over the second, and non-existent over the next 18 hours. This can be most clearly seen by following the crack growth from the left-most corner of the indent (white arrows).

For each indent, the number of primary cracks, secondary cracks, and circular cracks around the indent were counted. Primary cracks are defined as cracks originating from the corners of the Vickers indent and secondary cracks are cracks originating from one of the sides of the indent. The crack lengths and indent diagonals were measured under an optical microscope. Vickers hardness, and the average primary crack length were calculated. For indents made with the Fischer indenter, the loading/unloading curve for each indent was collected. The loading/unloading curves show the applied load (mN) versus indentation depth (μm) over the entire indentation cycle. From these curves the energies associated with the reversible and irreversible deformation components of the indentation process were calculated by integrating the areas underneath the curve. Reversible energy is the area under the unloading curve, while irreversible energy is the area under the loading curve minus the area under the unloading curve.

To study how the indentation behaviors change relative to the elastic properties of the glass, the transverse and longitudinal sound velocity were measured for each composition by ultrasonic pulse-echo technique using piezoelectric transducers (10 MHz range) and by Brillouin light scattering using a six-pass high contrast Fabry-Pérot interferometer. Density was measured by means of the Archimedes method using distilled water for the medium with an error of less than ±0.01 g/cm^3. Elastic moduli and Poisson's ratio were calculated from the sound velocity and the density of the glasses.

$$E = \rho V_T^2 (3V_L^2 - 4V_T^2)/(V_L^2 - V_T^2) \tag{1}$$

$$\mu = \rho V_T^2 \tag{2}$$

$$\nu = (V_L^2 - 2V_T^2)/2(V_L^2 - V_T^2) \tag{3}$$

$$K = E/(3(1-2\nu)) \tag{4}$$

where V_L and V_T are longitudinal and transverse sound velocities, ρ is sample density, E is Young's modulus, K is bulk modulus, μ is shear modulus, ν is Poisson's ratio. Brillouin values represent the average of five measurements taken across different points on a sample and have standard deviations of 0.7 GPa for Young's modulus, 0.7 GPa for bulk modulus, 0.4 GPa for shear modulus, and 0.006 for Poisson's ratio. Ultrasonic measurements are averages of two measurements made on a single sample, and varied by approximately 1.3 GPa for Young's modulus, 1.4 GPa for bulk modulus, 0.5 GPa for shear modulus, and 0.01 for Poisson's ratio. Thus, ultrasonic measurements for Young's modulus and shear modulus are precise enough to be used as a comparison to those from Brillouin light scattering, while Poisson's ratio values show too much variance.

The number of bridging oxygen per network former (Si or Ti) was calculated by assuming that the environment of Ti consists of four bridging oxygen atoms and one double-bonded oxygen that preferentially attracts a Na^+ ion [12,13] (see Fig. 2), so that

$$n_{BO} = (4([Si] + [Ti]) - ([Na] - [Ti]))/([Si] + [Ti]) \qquad (5)$$

which, according to the stoichimetry of the glass compositions, gives

$$n_{BO} = (4(1-x)-(2x-y))/(1-x) \qquad (6)$$

where x is the molar fraction of Na_2O and y is the molar fraction of TiO_2 in the glass.
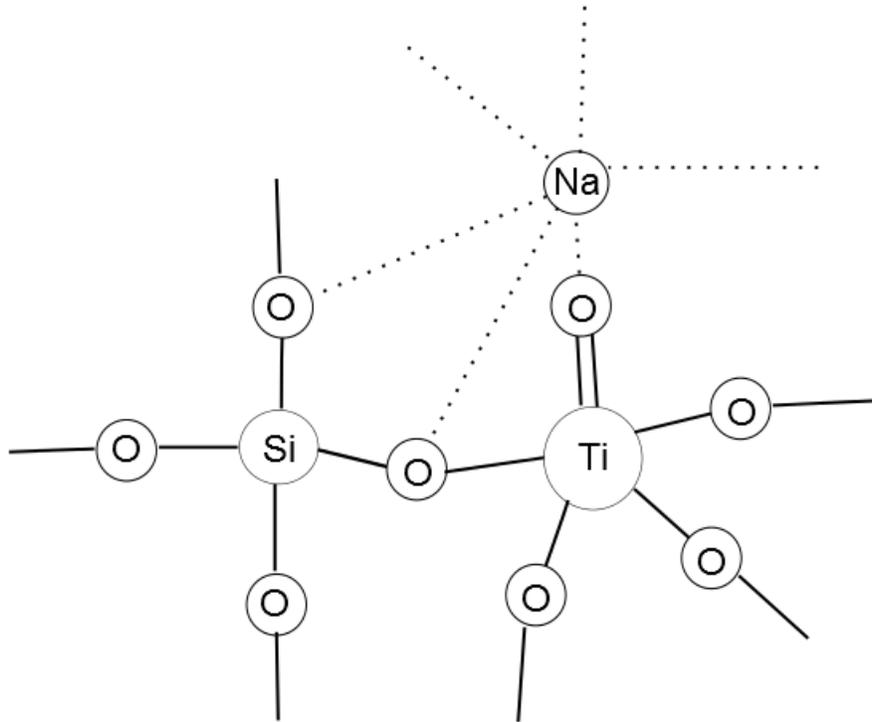

Fig. 2. Model structural units of Na_2O-TiO_2-SiO_2 glass at a titanium site, where Si forms four coordinated tetrahedra and Ti forms five-coordinated square pyramids.

Another important parameter is the glass atomic packing density (C_g), defined as the ratio between the minimum theoretical volume occupied by the ions and the corresponding effective volume of glass:

$$C_g = 1/\rho \ ((\Sigma f_i V_i)/(\Sigma f_i M_i)) \tag{7}$$

For the ith constituent with $A_x B_y$ chemical formula: $V_i = 4/3\pi N \ (x r_A^3 + y r_B^3)$, where N is Avogadro number, r_A and r_B are the ionic radii, ρ is the density, f_i is the molar fraction and M_i is the molar mass. The effective ionic radii in glass are usually not known with high accuracy. Shannon [14] tabulated the crystal radius and the effective ionic radius of halides and chalcogenides (including oxides). Whittaker [15] suggested using the mean of both values in the case of silicate glasses. An ab initio (i.e., when ρ is unknown) estimation of C_g can also be obtained by considering the density of the oxides used as constituents (as in Eq. (6)) to estimate the effective volumes from the mass and the corresponding density.

Glass transition temperatures were measured using differential thermal analysis (DTA) using a DTG-60 detector and a TA-60WS thermal analyzer. Prepared glasses were ground into a fine powder, added to platinum pans using alumina as a reference material. 50 mg of glass powder was used at each composition. Powders were heated from room temperature to 400 °C at 20 °C per minute and then from 400 °C to 800 °C at 10 °C per minute under a nitrogen atmosphere (25 ml/min). The onset, midpoint, and end of the glass transition range were found using the built-in function in the TA-60WS software.

Error in measured results is the standard deviation across the series of measurements taken whenever possible. Error in results calculated from measured results is the calculated variance assuming a covariance of zero. For theoretically calculated values, no error bars are shown. Error for the glass transition temperature is shown as the onset and end of the glass transition range, as this is larger than error between measurements. Error in the critical load to initiate cracks was estimated using a fitting method and is described in the results in more detail.

3. Results

Indentation micrographs for the twelve Na_2O-TiO_2-SiO_2 glasses are shown in Figs. 3-6. At 49 N (Fig. 3), all samples exhibit radial-median cracks. Samples with 10 mol% Na_2O also appear to have cone/ring cracks, while 15, 20, 25 mol% Na_2O samples have lateral cracks, as exhibited by the lack and presence of chipping and birefringence patterns, respectively. As the load is decreased, cone/ring cracking disappears almost immediately, with slight signs of it in the $10Na_2O$-$4TiO_2$-$86SiO_2$ sample at 9.8 N. Radial-median and lateral cracks appear to shrink relative to indent diameter as load decreases. Samples with 10% Na_2O and 25% Na_2O appear most resistant to crack initiation, with some samples beginning to show less than four cracks at 4.9 N. Crack length appeared to increase with increasing Na_2O content, particularly visible at 2.9 N in Fig. 6.
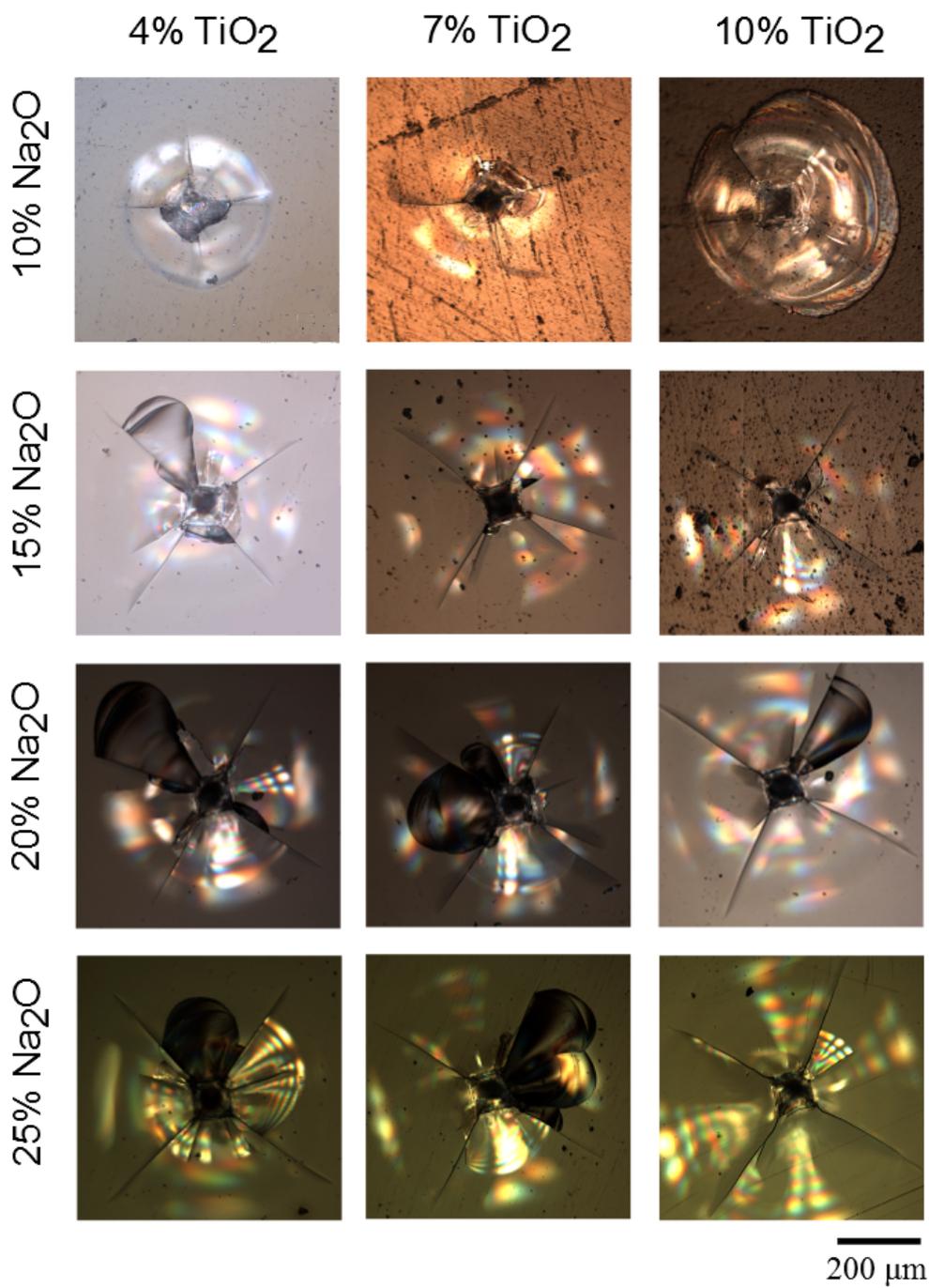
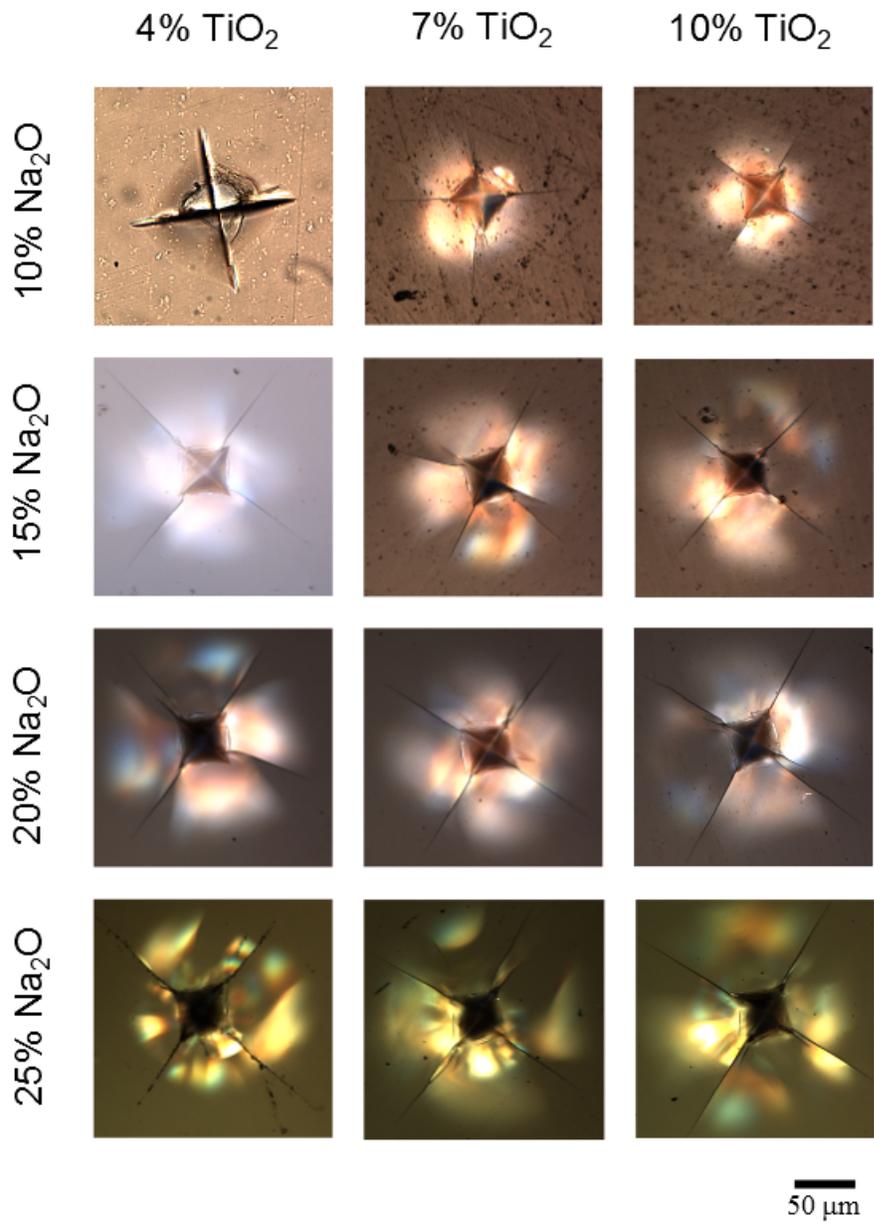**Fig. 3.** Vickers indentations performed at 49 N on Na_2O-TiO_2-SiO_2 glasses.

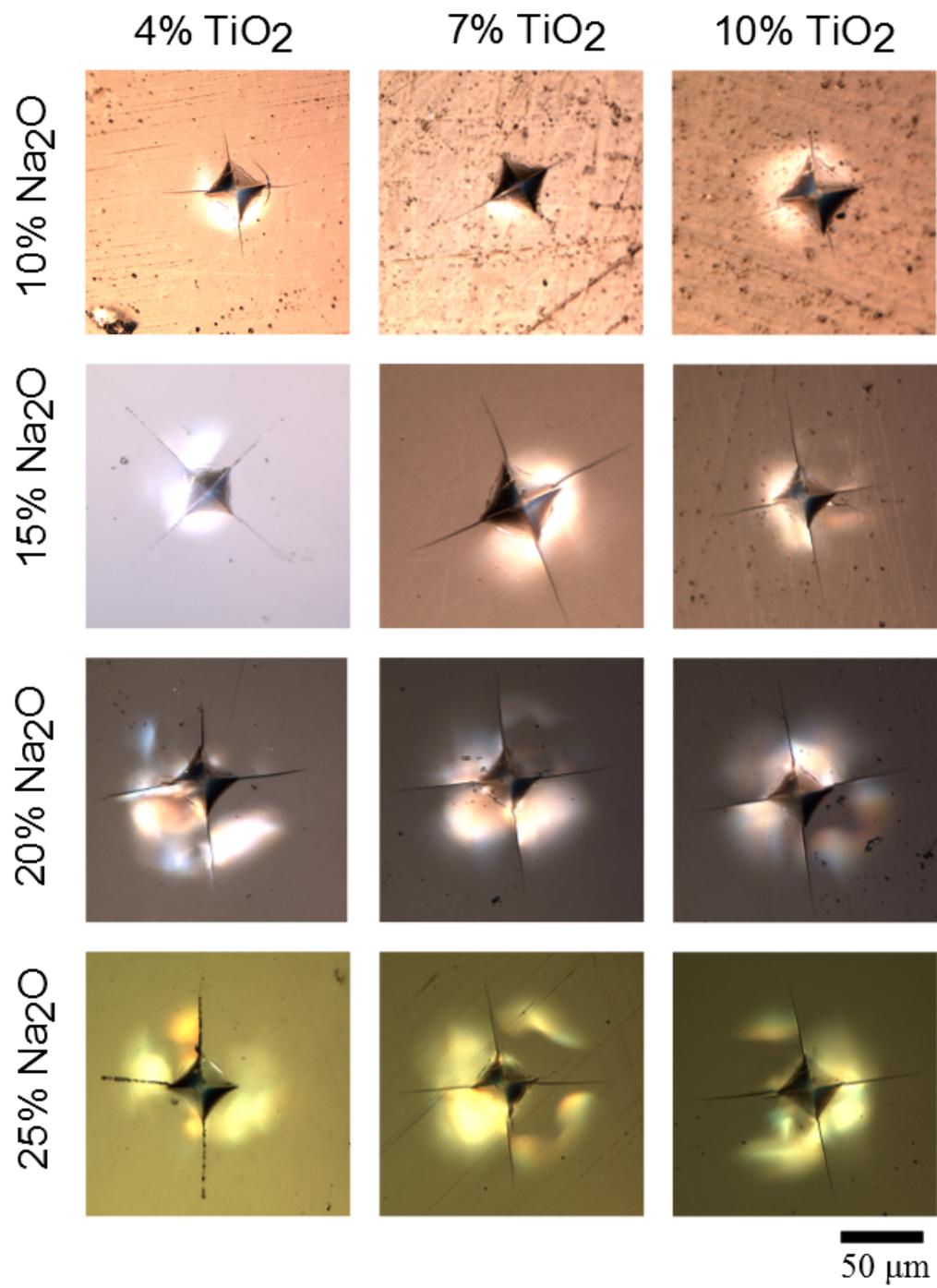**Fig. 4.** Vickers indentations performed at 9.8 N on Na_2O-TiO_2-SiO_2 glasses.

Fig. 5. Vickers indentations performed at 4.9 N on Na_2O-TiO_2-SiO_2 glasses.

Fig. 6. Vickers indentations performed at 2.9 N on Na_2O-TiO_2-SiO_2 glasses.

Fig. 7 shows representative cracking patterns for all samples across loads tested. The number of cracks originating from each indent was averaged across the ten indents examined for each load and composition according to the following categories: radial-median cracks starting at the four corners of the indent; radial-median cracks starting from anywhere other than the four

corners; and ring/cone cracking or chipping around the indent. All samples showed a good resistance to cracking relative to the wide range of compositions previously studied by Sellapan et al. [16]. In the 10% Na_2O samples ring/cone cracking is present, while chipping occurs for all the other compositions. Fig. 7 is only intended to show average crack initiation, and does not represent indent size or crack length. Glasses initially become more susceptible to cracking with increasing Na_2O content from 10% to 20%, before quickly become less susceptible at 25% Na_2O. TiO_2 appears to have an effect of making glass more susceptible to cracking that is dependent on the Na_2O concentration. At 10% Na_2O increasing the TiO_2 content does not appear to have a noticeable effect on crack initiation. Some increase in susceptibility to cracking is observed at 15% and 20% Na_2O, but at 25% Na_2O increasing TiO_2 concentration significantly decreases the load required for cracking.

Fig. 7. Cracking patterns around Vickers indentations in Na_2O-TiO_2-SiO_2 glasses over a range of loads. Compositions are in mol percent. Cracking patterns shown represent an average of ten indents and show the average number of primary, secondary, and circular cracks. Indents made

at 49, 9.8, 4.9, and 2.9 N were studied under an optical microscope, at 1 and 0.5 N were studied under SEM.

Hardness values and the contribution of reversible (elasticity based) and irreversible deformation to the energy from indentation tests are shown in Table 1. Hardness values were calculated using the indentation load and the surface area of the indentation, averaged across ten indents. The standard deviation of hardness values is approximately 0.5 GPa. The hardness measurements show a slight load dependence, increasing as the load is decreased (as is typically the case and referred to as the Indentation Size Effect). Hardness appears to decrease with increasing Na_2O content and increase with increasing TiO_2 content. The elastic and permanent components of the deformation energy were calculated using the indentation loading and unloading curves and are expressed as fractions of the total work required to create the indent. The permanent and elastic components of the indentation deformation energy do not show load dependence. Values presented in Table 1 are averages of measurements taken at 1 N, 0.5 N, and 0.1 N and have a standard deviation of 0.7%. There appears to be a slight increase in the permanent energy component as the fraction of SiO_2 in the glass decreases until around 70%, where it starts to decrease again.

Table 1 Hardness and indentation energy of Na_2O-TiO_2-SiO_2 glasses for indentations made at six different loads. Error is given as the standard deviations.

Composition	Hardness (GPa)						Deformation Energy	
Na_2O-TiO_2-SiO_2	49 N	9.8 N	4.9 N	2.9 N	1 N	0.5 N	Reversible (%)	Permanent (%)
10-4-86	3.8±0.6	5.7±0.8	6.3±0.8	5.5±0.2	5.0±0.4	6.0±0.5	58.8±0.1	41.2±0.1
10-7-83	4.8±0.4	4.7±0.4	4.8±0.1	6.6±0.2	5.9±0.4	5.1±0.4	56.6±0.6	43.4±0.6
10-10-80	5.4±1.0	5.9±0.4	5.3±0.2	5.8±0.2	6.7±0.3	6.2±0.2	58.2±0.5	41.8±0.5
15-4-81	5.5±0.7	5.9±0.2	6.2±0.2	6.6±0.2	5.7±0.9	5.1±0.3	58.6±1.0	41.4±1.0
15-7-78	4.7±0.3	4.9±0.2	4.9±0.1	5.1±0.2	5.7±0.1	6.2±0.2	56.5±0.9	43.5±0.9
15-10-75	4.4±0.9	5.4±0.3	5.2±0.3	5.7±0.2	5.8±0.1	6.3±0.2	55.5±0.7	44.5±0.7
20-4-76	4.5±0.5	4.5±0.2	4.4±0.2	4.9±0.1	5.0±0.1	5.1±0.1	54.9±0.9	45.1±0.9
20-7-73	4.7±0.3	4.9±0.1	5.0±0.2	5.3±0.2	5.5±0.3	5.8±0.5	54.9±1.0	45.1±1.0
20-10-70	4.5±0.2	4.8±0.2	5.0±0.2	5.2±0.3	5.1±0.5	5.7±0.3	53.9±0.5	46.1±0.5
25-4-71	4.2±0.3	4.2±0.3	4.2±0.2	4.2±0.3	4.9±1.3	4.7±0.1	55.4±1.4	44.6±1.4
25-7-68	4.5±0.1	4.4±0.2	4.6±0.2	4.7±0.2	4.1±0.1	5.3±0.4	55.0±0.9	45.0±0.9
25-10-65	4.4±0.3	4.6±0.2	4.7±0.3	4.9±0.1	5.5±0.7	5.3±0.2	56.2±0.3	43.8±0.3

The crack resistance of a glass can be found by plotting the average number of cracks as a function of load [10]. A linear relationship was observed between the log of the indentation load and the number of cracks up to the maximum of four primary cracks. Crack resistances were calculated using logarithmic fits using the points between the maximum load at which zero cracks were observed and the minimum load where four cracks were observed. Error in the crack resistances were approximated using the same fitting method except using a number of cracks one standard deviation above average and one standard deviation below average. When adding or subtracting standard deviations, the number of cracks was still limited to a maximum of 4 and a minimum of 0. These restrictions create non-symmetrical error bars. Table 2 shows

the crack resistance of the glasses examined as the loads required to generate up to four cracks around a Vickers indent. Due to the relatively large increase in load between 2.9 N, 9.8 N, and 49 N, predictions for the minimum load when four cracks will be generated can be expected to be less accurate for samples for which four cracks were only observed above 2.9 N. The load to generate cracks appears to decrease with decreasing SiO_2 content up to 70-76% SiO_2 before increasing again.

Table 2 The minimum load required to generate a given number of cracks around a Vickers indent for $Na_2O-TiO_2-SiO_2$ glasses. The zero cracks column represents the maximum load at which no cracks could be detected (SEM and Optical microscope) at the corners of a Vickers indent.

Composition	Minimum load to generate cracks (N)				Maximum Load (N)
$Na_2O-TiO_2-SiO_2$	4 Cracks	3 Cracks	2 Cracks	1 Crack	0 Cracks
10-4-86	4.6	2.8	1.6	0.8	0.54
10-7-83	10.5	6.3	3.2	1.4	0.76
10-10-80	5.7	3.4	1.8	0.84	0.51
15-4-81	14.7	4.3	2.9	1.0	0.50
15-7-78	2.9	1.8	1.1	0.65	0.50
15-10-75	1.1	0.9	0.75	0.60	0.44
20-4-76	1.2	1.0	0.81	0.61	0.42
20-7-73	2.9	1.2	0.50	0.20	0.08
20-10-70	2.9	2.1	1.4	0.74	0.15
25-4-71	9.8	7.2	5.1	3.5	2.6
25-7-68	2.9	2.5	2.0	1.5	1.0
25-10-65	9.8	6.7	4.5	3.3	2.9

Values for Young's modulus, bulk modulus, shear modulus, and Poisson's ratio measured using Brillouin light scattering [17] and ultrasonic pulse techniques [4] are shown in Table 3. Values for elastic moduli measured through Brillouin light scattering tend to be slightly higher than those measured through the ultrasonic pulse technique, with the exception of the 25 Na_2O glasses. This can be tentatively associated with the volume of glass being measured and the acoustic wavelength used to measure that volume. Brillouin light scattering has a spot size on the order of tens of microns while the ultrasonic method measures across a sample approximately 1 cm x 1 cm x 0.4 cm. Additionally, Brillouin light scattering has an acoustic wavelength of ~0.5 μm while ultrasonic resonance has an acoustic wavelength of 0.05-10 mm. Thus the ultrasonic measurements are more likely to include any defect in the volume measured, such as small bubbles or microcracks, and for these defects to alter the measured acoustic velocities.

Table 3 Elastic properties of Na_2O-TiO_2-SiO_2 glasses as measured by Brillouin light scattering and by ultrasonic pulse techniques. Error for Brillouin measurements is the standard deviation across ten measurements. E is Young's modulus, K is bulk modulus, μ is shear modulus, and ν is Poisson's ratio.

Composition	E (GPa)		K (GPa)		μ (GPa)		ν	
Na_2O-TiO_2-SiO_2	Brillouin ±0.7	Ultrasonic ±1.3	Brillouin ±0.7	Ultrasonic ±1.4	Brillouin ±0.4	Ultrasonic ±0.5	Brillouin ±0.006	Ultrasonic ±0.01
10-4-86	68.2	65.3	35.7	38.2	28.9	26.9	0.182	0.215
10-7-83	71.0	70.4	37.3	38.8	30.0	29.4	0.183	0.198
10-10-80	71.8	71.8	39.4	39.0	30.0	30.1	0.196	0.194
15-4-81	68.2	66.1	38.3	36.9	28.4	27.5	0.203	0.201
15-7-78	69.3	68.3	39.8	41.1	28.6	27.9	0.210	0.224
15-10-75	71.2	69.3	41.9	40.4	29.3	28.6	0.217	0.214
20-4-76	64.6	63.9	40.2	39.8	26.2	25.9	0.232	0.232
20-7-73	67.7	65.8	41.8	41.5	27.5	26.6	0.230	0.236
20-10-70	69.8	67.3	43.9	47.7	28.3	27.6	0.235	0.222
25-4-71	64.2	66.3	40.4	34.2	26.0	28.0	0.235	0.184
25-7-68	69.1	70.9	43.6	37.4	28.0	29.7	0.236	0.192
25-10-65	69.2	73.4	43.9	40.7	27.9	30.3	0.237	0.212

Young's modulus consistently increases with increasing TiO_2 concentration and generally decreases with increasing Na_2O content. Shear modulus also increases with increasing TiO_2 concentration, but shows less of a decrease with increasing Na_2O concentration. Bulk modulus increases with both TiO_2 and Na_2O concentration. Poisson's ratio increases slightly with increasing TiO_2 concentration and strongly with increasing Na_2O content. The change in Poisson's ratio is less noticeable between the 20% Na_2O series and the 25% Na_2O series.

4. Discussion
4.1 Network connectivity and elasticity

The calculated n_{BO} ranges from 3.3 to 4 and brings to light some interesting correlations between the atomic structure and the mechanical properties. Increases in the n_{BO} result from either an increase of the TiO_2/SiO_2 ratio or a decrease of the sodium content at a given TiO_2/SiO_2 ratio, but while a decrease of the sodium content results in a decrease of ν (as expected in regard of the decrease of the atomic packing efficiency), an increase of the titanium content induces an opposite effect, i.e. ν increases, suggesting a better atomic packing even though Ti is playing the role of a glass network former. The overall decrease of ν with increasing n_{BO} (Fig. 8), especially for $n_{BO}>3.6$, would corroborate the increase in the cross-linkage of the atomic network, making shear more difficult with respect to volume change (ν scales with K/μ, where K and μ are bulk and shear modulus, respectively).
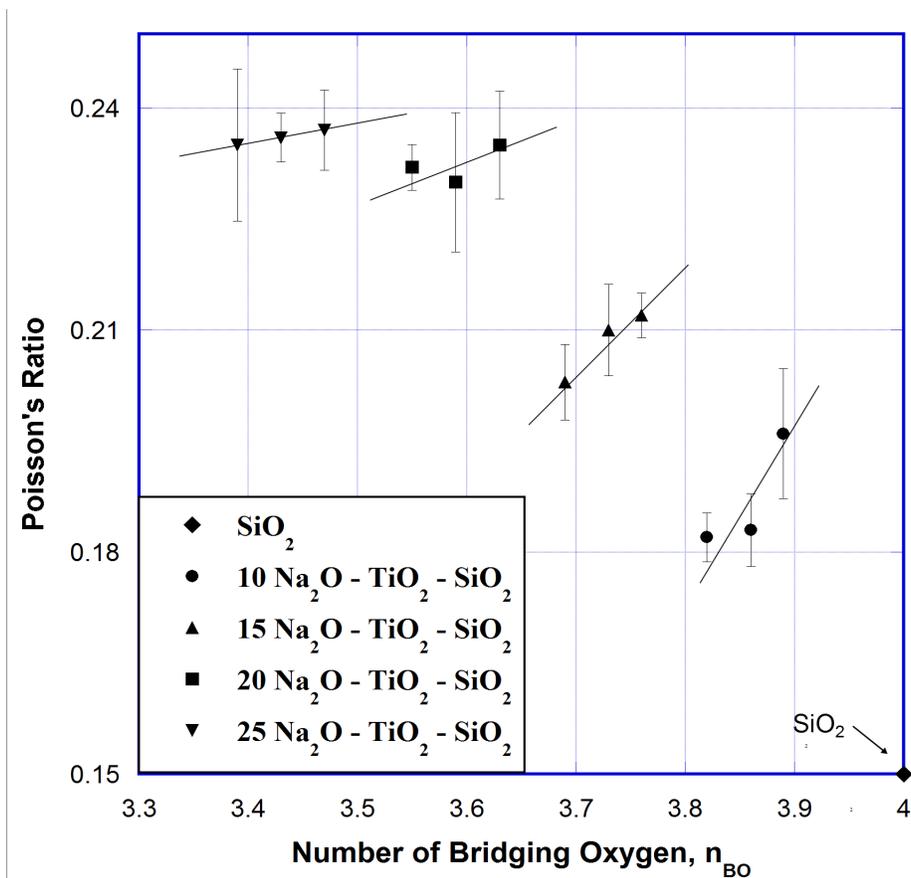

Fig. 8. Number of bridging oxygen per (Si,Ti)-centered tetrahedron versus Poisson's ratio measured through Brillouin light scattering. Error bars represent standard deviation across ten measurements. TiO_2 content increases from 4 to 10 percent moving from left to right for at each Na_2O content. Lines are provided as guides for the eyes.
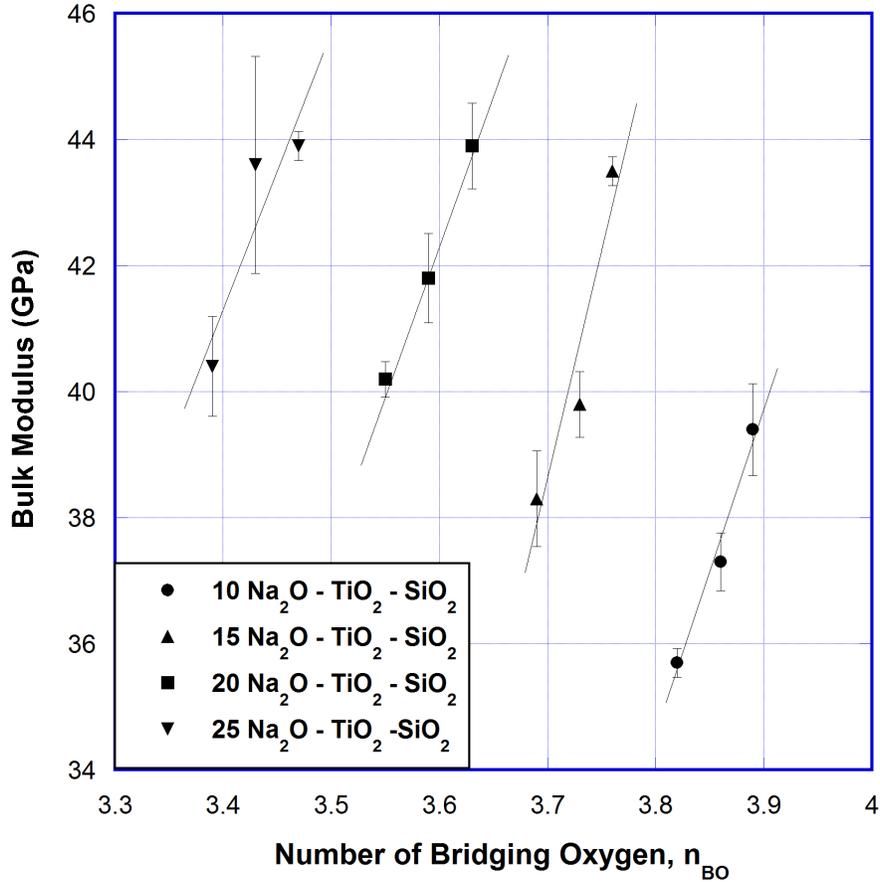
Fig. 9. Bulk modulus as obtained by Brillouin light scattering as a function of the number of bridging oxygen atoms per (Si,Ti)-centered tetrahedron. Lines are provided as guides for the eyes. TiO_2 content increases from 4 to 10 percent moving from left to right for at each Na_2O content.

The bulk modulus (as obtained by Brillouin light scattering) is given as a function of the TiO_2/SiO_2 ratio (number of bridging oxgen) for series at fixed sodium content in Fig. 9. Interestingly, in this ternary system, sodium has little influence on K, especially at large Ti content (for instance glasses with 10% TiO_2 have almost identical K values, between 43 and 44 GPa regardless of the sodium content), whereas at a given sodium content K markedly increases with TiO_2/SiO_2. Following Grüneisen [18] and previous reports focusing on glasses of a wide range of compositions [4,19,20], K, being expressed in Pa (i.e., J/m^3) can be viewed as a volume density of energy. For a multi-constituent glass, the volume density of energy (dissociation enthalpy per unit volume) can be roughly estimated from the properties of the constituents (Fig. 10) according to

$$<U_o/V_o>=\Sigma f_i \Delta H_{ai}/(\Sigma f_i M_i/\rho_i) \tag{7}$$

where ρ_i is the density, and f_i and M_i are the molar fraction and the molar mass, respectively. For the ith constituent written as A_xB_y, according to an ordinary Born-Haber cycle:

16

$$\Delta H_{ai} = x \, \Delta H^o_f(A,g) + y\Delta H^o_f(B,g) - \Delta H^o_f(A_xB_y) \tag{8}$$

where ΔH_{ai} is the formation enthalpy of the glass component A_xB_y, $\Delta H^o_f(A,g)$ is the standard formation enthalpy of the cation (A_x), $\Delta H^o_f(B,g)$ is the standard formation enthalpy of the anion (B_y), and x and y are the amounts of elements A and B in the glass components, respectively.
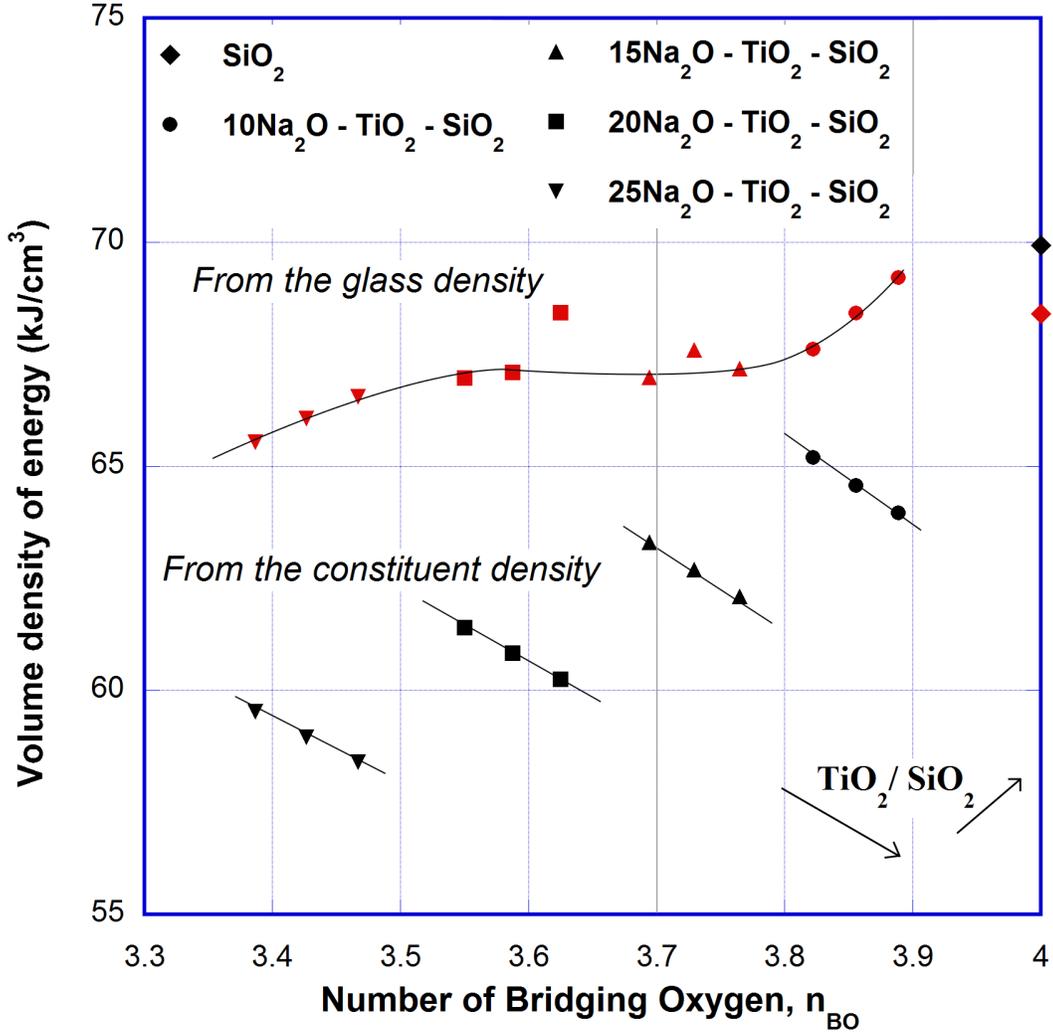

Fig. 10. Volume density of energy as estimated from thermochemistry data using the actual molar volume for the glass (from the experimental density; red symbols) or the molar volume calculated from the density of the constituents as a function of the number of bridging oxygen atoms per (Si,Ti)-centered tetrahedron (black symbols). Lines provided as guides for the eyes. Arrows indicate the direction of increasing TiO_2 or SiO_2 respectively.

The standard formation enthalpy of a cation is equal to its sublimation enthalpy; whereas, for an anion, gaseous in its standard state, the molar dissociation energy of the gas molecules must be considered. The denominator in the right hand side of Eq. (7) represents the whole volume occupied by the atoms of an "equivalent" mole of glass, provided the volume occupied by each atom is the same as in the crystal of the raw material of each component of the glass.

The presence of free volume in the glass and the fact that inter-atomic distances, angles and coordination numbers in the glass network differ from those in the crystalline compounds, is thus not taken into account in this *ab initio* approach. The actual trends might thus differ from the predicted ones and this provides interesting information relevant to the glass network structure. For instance, the actual increase of K with the titania content (Fig. 9), which contrasts with the prediction from the constituent, is thus consistent with the fact that TiO_2 is efficient to increase ν (Fig. 8), as well as the network energy as illustrated by the steep rise of T_g as a function of the TiO_2/SiO_2 ratio (number of bridging oxygen) for given Na_2O series (Fig. 12). Note that i) T_g is less sensitive to changes in the sodium content than it is to the titanium content (Fig. 12); and ii) titanium tends to tighten the atomic network, so that $<U_o>/<V_o>$ increases whereas a decrease of the volume density of energy was expected from the density and thermochemistry of the starting oxides. The role of titanium is quite unusual. The atomic packing density is generally found to decrease as a glass becomes richer in glass-forming elements (because a highly cross-linked network follows with less room for the flexibility required for good packing). The present analysis suggests that the environment and bonding strength of titanium in the glass significantly differs from the one in the crystalline titanium oxide.
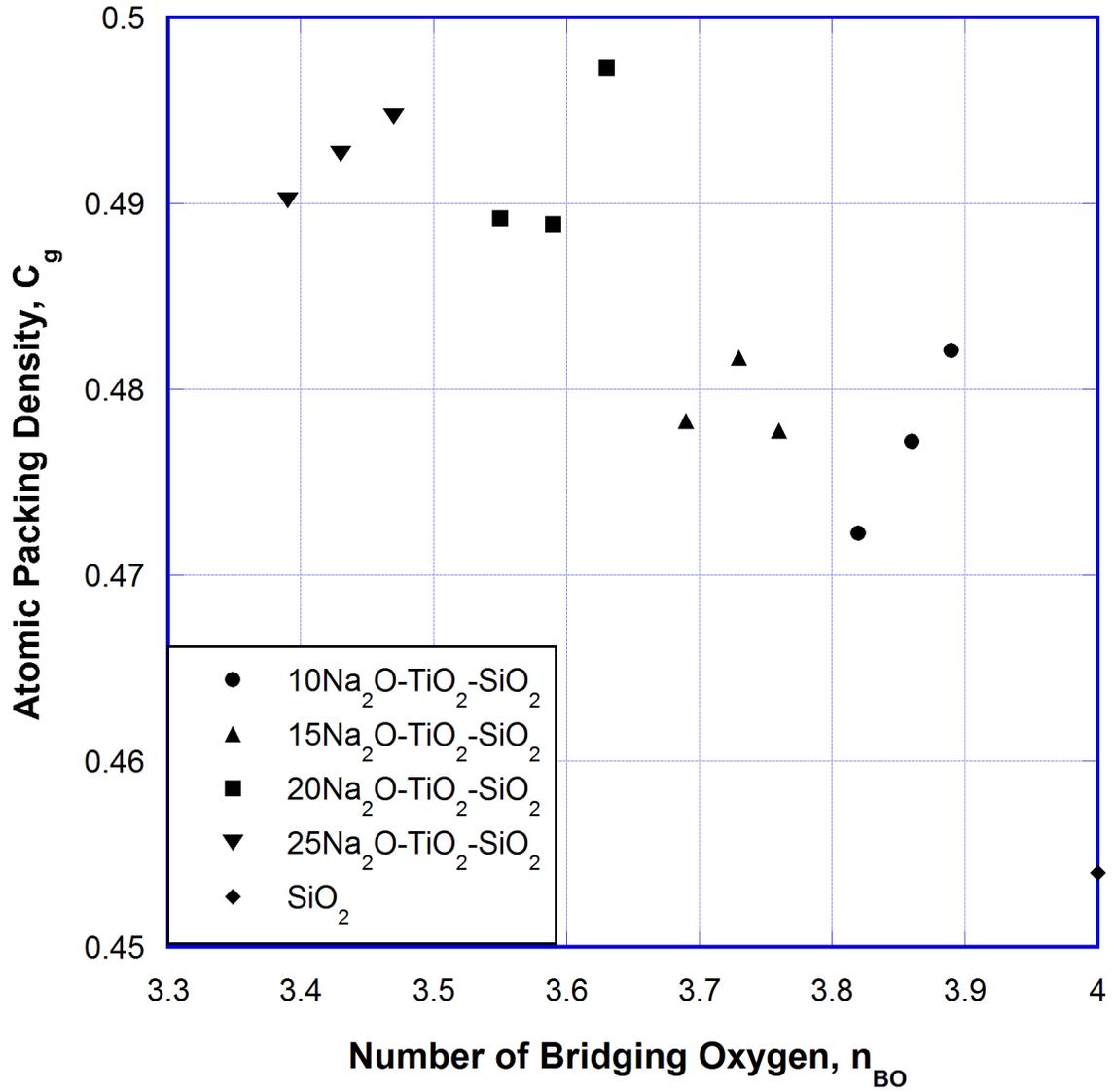
Fig. 11. Atomic packing density (defined in Eq. 6) as a function of the number of bridging oxygen atoms per (Si,Ti)-centered tetrahedron. TiO_2 content increases from 4 to 10 percent moving from left to right for at each Na_2O content.
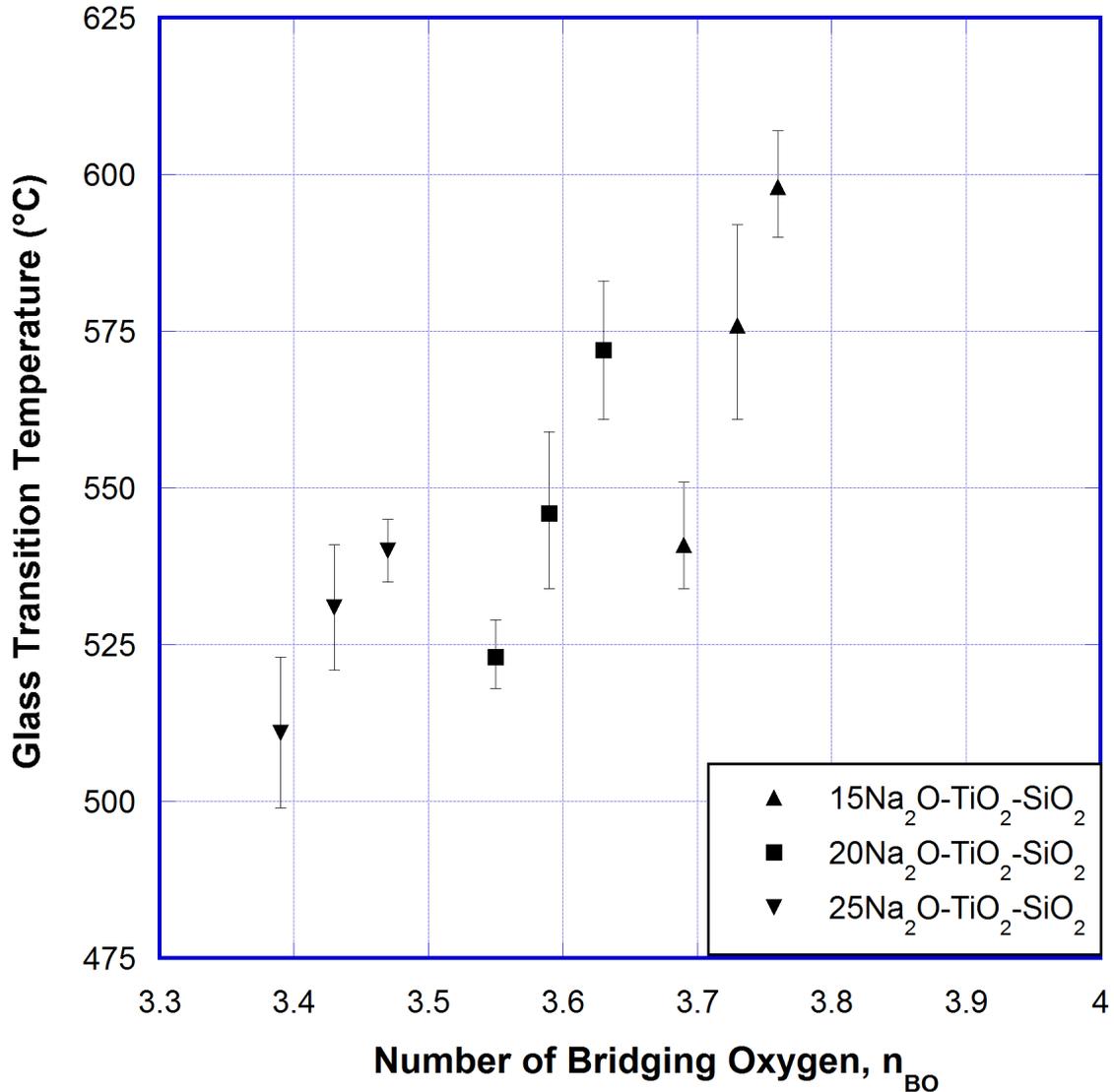
Fig. 12. Glass transition temperature (from DTA) as a function of the number of bridging oxygen atoms per (Si,Ti)-centered tetrahedron. TiO_2 content increases from 4 to 10 percent moving from left to right for at each Na_2O content. Temperatures plotted are the midpoint of the glass transition, and error bars represent the onset and end of the glass transition.

The bonding environment in soda-titania-silica glasses has been studied previously through X-ray absorption near edge structure (XANES) and extended X-ray absorption fine structure (EXAFS). Henderson and Fleet observed a mixture of [4]Ti and [5]Ti in Na_2SiO_3-TiO_2 glasses [20]. Farges et al. has published numerous studies on the role of Ti in the structure of a variety of glasses [12,13,22,23] and found that in Na_2O-TiO_2-SiO_2 glasses [5]Ti made up more than 80% of the Ti in the glasses. [5]Ti takes a square pyramidal geometry with four Ti-O bonds and one T=O bond. These bonds were found to have lengths of approximately 1.91 Å and 1.7 Å and valences of approximately 0.7 v.u. and 1.7 v.u., respectively. Bond valences are given in valence units and were calculated using the relationship of Brown and Altermatt [13].

20

Because of the large differences in bonding energies (Ti-O versus Ti=O) and bond distances suggested by neutron scattering, a percolation model where Ti occupied positions between regions relatively rich in Na and those relatively poor in Na has been suggested [13]. [5]Ti was proposed to act as both a network modifier and a network former. Simply considered as a network former, such as how it behaves in pure titanium oxide, we would expect it to open the structure, reduce the packing density, and lower the volume density of energy. As the observed result is entirely opposite (Figs. 10 and 11), the role of Ti as a network modifier must have a significant impact on the medium range structure in the glass.

4.2. Indentation cracking

As the titania content decreases or the sodium oxide content increases, the number of bridging oxygen decreases and the atomic packing density increases in the glass, and it is expected that the primary inelastic indentation deformation mechanism will shift from densification to shear flow. This shift is expected to be accompanied by a change in the cracking behavior. In pure silica we expect median-radial cracks and some ring cracking depending on the indentation load. Na has a strong effect of decreasing the number of bridging oxygen and increasing the atomic packing density. This should decrease the driving force for ring/cone cracking and increase the driving force for lateral cracking [11]. It may decrease the driving force for radial-median cracks as well.

Ti as a network former with a weaker bond strength than Si would be expected to increase the glass's susceptibility to cracking. However, in the presence of Na, titania strengthens the glass (Table 3). A possible explanation, using the model proposed by Farges et al. [13], would be that the Ti promotes some local ordering in the glass and preferentially attracts Na, reducing the effective number of non-bridging oxygen in the silica tetrahedral network. Ti increases both the atomic packing density and stiffens the network. It is unclear which of these properties will have the stronger effect on the cracking behavior of the glass; however, it is reasonable to expect a shift from densification to shear flow for the deformation mechanism.

Driving forces for different cracking modes are shown in Fig. 13. The lines for each cracking mode show where the driving force for the mode is zero, and pluses and minuses indicate that the driving force is either tensile or compressive, respectively. Error bars in E/H values is the variance calculated from standard deviations in Young's modulus and hardness assuming covariance is zero. Details for the calculation of the driving forces for cracking (accounting for the elastic recovery) is given in [11].
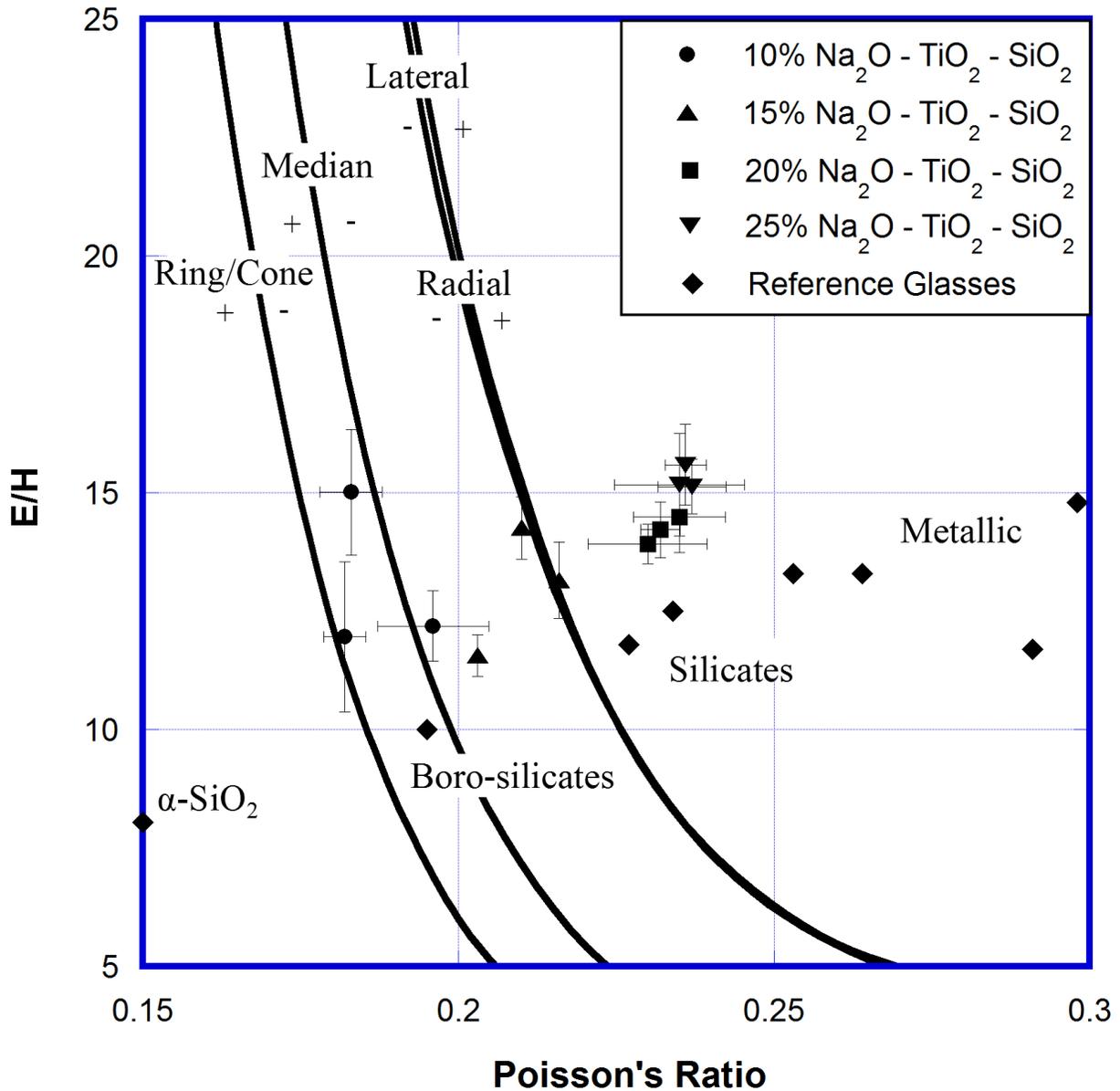
Fig. 13. Plot of Young's modulus (GPa) over hardness (GPa) versus Poisson's ratio. E/H provides a unitless measure of a material's resistance to deformation that combines elastic and plastic stiffnesses. Lines represent the transition from tensile (+) to compressive (-) driving forces for different cracking modes. Calculation of these stresses and data for the reference glasses can be found in [11].

The ratio of elastic modulus over hardness and Poisson's ratio is necessary information to predict the driving force for cracking using the Boussinesq stress field [24]. As seen in Figs. 3-6, changes in the soda concentration strongly promote radial and lateral cracking over median and ring/cone. Ring/cone cracking was only seen in the 10% Na_2O samples and only at high loads, which matches the driving force predictions reasonably well. As TiO_2 and Na_2O concentrations

are increased and Poisson's ratio shifts to higher values, it would be expected that radial and lateral cracks would become more prominent and cone/ring cracking would disappear.

4.3 Indentation deformation and hardness

Plot of the critical loads to generate two and four cracks around an indent versus Poisson's ratio reveals an unexpected trend (Fig. 14). As Poisson's ratio is increased, the load required to create cracks in the glass initially decreases quickly until it reaches a minimum at approximately $\nu = 0.22$ (worse case in terms of visible crack initiation resistance). Further increasing Poisson's ratio above $\nu = 0.23$ results in a sharp increase in the critical crack initiation load. This behavior is not predicted by the driving force calculations shown in Fig. 13, which suggest that the driving force for radial cracks should continue increasing as Poisson's ratio is increased. The observed behavior could be explained by a change in the deformation behavior in the glass. At low Poisson's ratio, the primary mode of deformation is densification, while as Poisson's ratio increases, a shift from densification to shear flow is expected, as is observed for instance as one moves from oxide glasses to metallic ones. At intermediate Poisson's ratio neither densification nor shear flow dissipate the stresses sufficiently to prevent cracking. The deformation mechanism and the fracture toughness are both likely to depend on the composition of the system, and a significant increase of K_{IC} might compensate for the rise of the driving force for indentation cracking (currently under study).
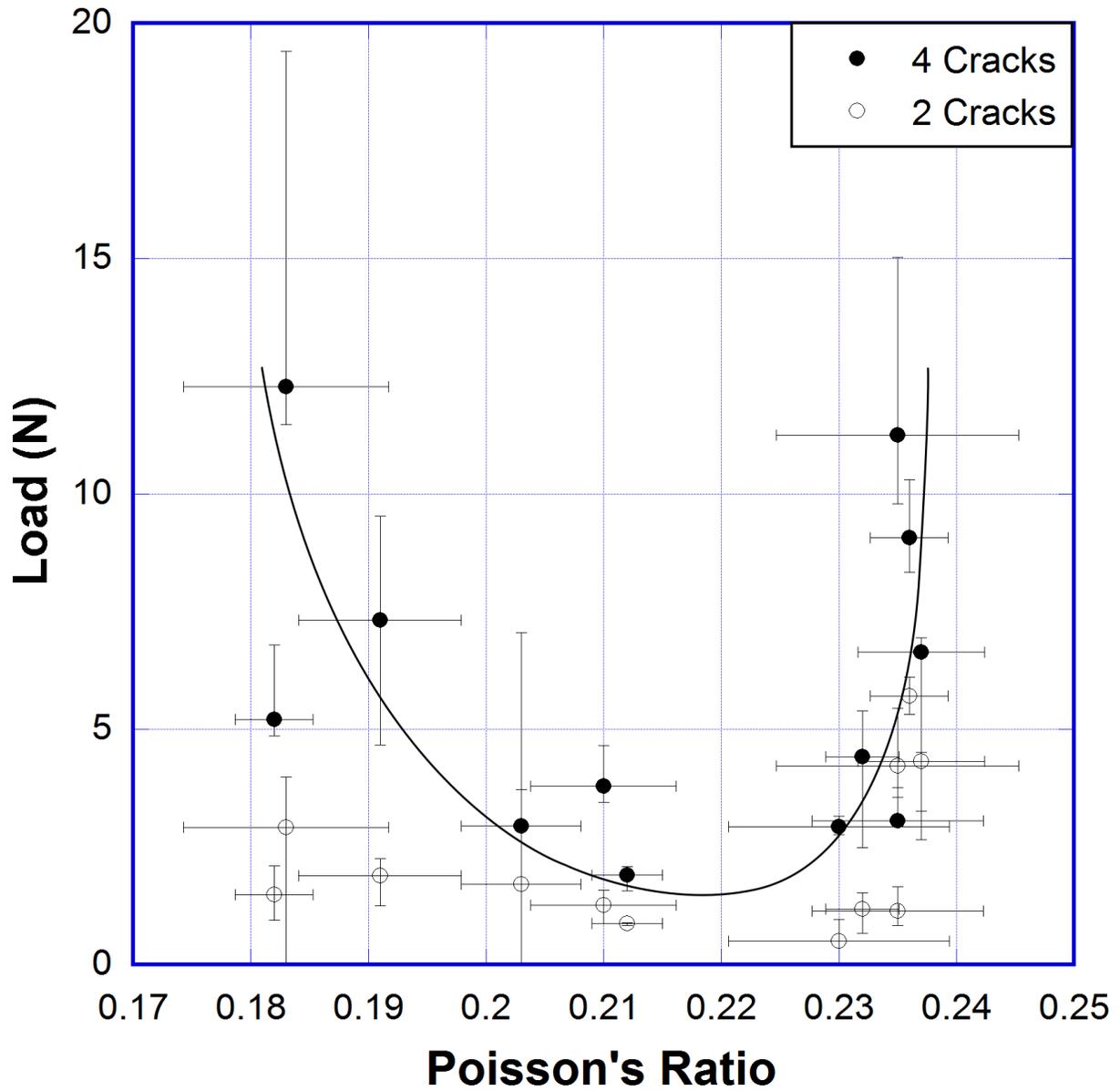
Fig. 14. Critical load to create cracks around a Vickers indent versus Poisson's ratio measured by Brillouin light scattering. Poisson's ratio values are averages of ten measurements. Line provided as a guide for the eyes through data points for 4 cracks.
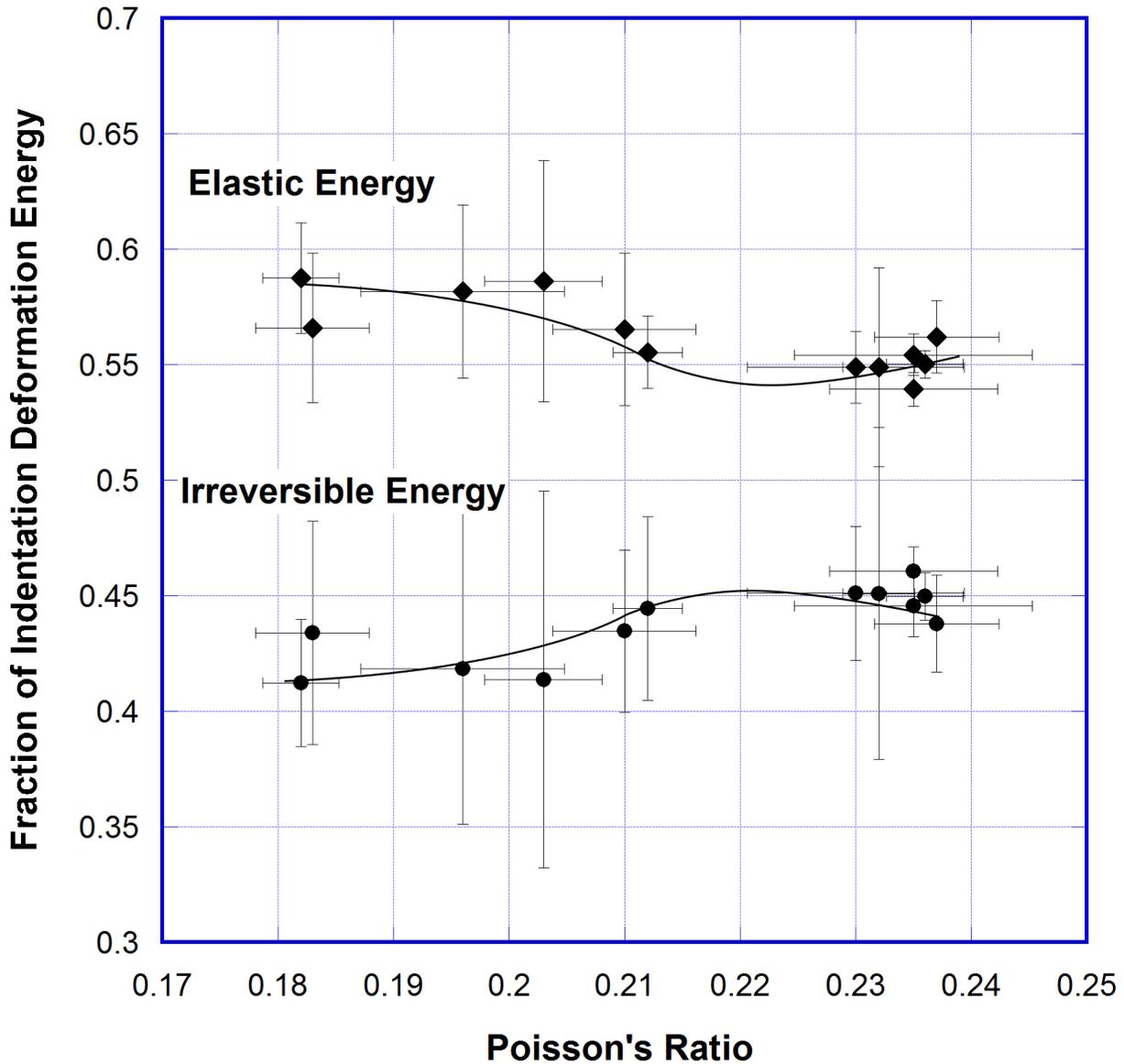
Fig. 15. Reversible and permanent fractions of the energy required to create an indent versus the number of bridging oxygen for $Na_2O-TiO_2-SiO_2$ glasses. Energies were determined using the loading and unloading curves of indentations at 1 N, 0.5 N, and 0.1 N, with 10 indents at each load. No dependence on load was observed for the relative fractions of plastic and elastic energy. Lines are provided as guides to the eyes.

This result is peculiar, because the indentation energy loss associated with the irreversible deformation process exhibits a bell-shape curve as a function of Poisson's ratio, with a maximum at $\nu \approx 0.21-0.23$ corresponding to the range where the critical load for cracking is minimum (Fig. 15). One would expect that the resistance to cracking should increase with the amount of dissipated energy by means of irreversible processes ("plastic" deformation). However, it seems from a comparison between the bell-shape energy and the U-shape critical load curves that the increase of the dissipated energy coincides to the building-up of residual stresses, possibly because shear flow combined with densification in this range results in the displacement of

matter downward, to produce an elastically constrained axisymmetric region. Further investigations are required to get more insight into this phenomenon. Two hypothesis can be invoked, namely

i) Fracture toughness comes into play in the initiation of cracking and might change with composition in such a way that K_{IC} is larger as ν increases to 0.23. Crack initiation might be further retarded thanks to the ease for irreversible flow in this ν range (as per the irreversible indentation energy plot)

ii) As ν increases, the indentation cracking pattern evolves toward more lateral and radial cracking, and Palmqvist cracking prevail, so that the available mechanical energy might dissipate through the formation of more and longer radial cracks (for a given fracture area, the depth being smaller, cracks must be longer).

It has been shown that the crack resistance of glasses is strongly affected by the humidity present during the indentation process [25]. In this study humidity was not controlled during indentation experiments. Its effect on the critical crack initiation load will be investigated in our future study. Humidity seems unlikely to affect the fractions of permanent and elastic deformation energy at loads, which were measured at loads where cracking did not occur.

5. Conclusion

Our study shows that TiO_2 has a striking tightening effect on the glass network, increasing both the packing density and the network energy. This is expressed in the measured elastic properties by an increase in Young's modulus and Poisson's ratio. In regard to a previously reported indentation-damage map, Na_2O-TiO_2-SiO_2 glasses turn out to fall in the property range (E/H, ν) where the driving force for indentation cracking, whatever the cracking pattern of concern (radial, median, lateral), is relatively limited and exhibit a good indentation damage resistance, especially for the $15Na_2O$-$4TiO_2$-$81SiO_2$ and $25Na_2O$-$4TiO_2$-$71SiO_2$ compositions. A minimum in the critical crack initiation load was observed in the range of $\nu = 0.21$-0.22.

References

[1]   J. Lewandowski, W. Wang, A. Greer, Intrinsic Plasticity or Brittleness of Metallic Glasses, Philos. Mag. Lett. 85 (2005) 77–87.

[2]   S.F. Pugh, Relations between the Elastic Moduli and the Plastic Properties of Polycrystalline Pure Metals, Philos. Mag., 45 (1954) 823-843.

[3]   T. Rouxel, H. Ji, J. Guin, F. Augereau, B. Ruffle, Indentation Deformation Mechanism in Glass: Densification versus Shear Flow, J. Appl. Phys. 107 (2010) 094903.

[4]   T. Rouxel, Elastic Properties and Short-to Medium-Range Order in Glasses, J. Am. Ceram. Soc. 90 (2007) 3019–3039.

[5]   Y.H. Liu, G. Wang, R.J. Wang, D.Q. Zhao, M.X. Pan, and W.H. Wang, Super plastic bulk metallic glasses at room temperature, Science, 315 (2007) 1385-1388.

[6]   M.D. Demetriou, M.E. Launey, G. Garrett, J.P. Schramm, D.C. Hofmann, W.L. Johnson, and R.O. Ritchie, A damage-tolerant glass. Nature Materials, 10 (2011) 123-128.

[7]   M. Wada, H. Furukawa, K. Fujita, Crack Resistance of Glass on Vickers Indentation, Proc. Xth I.C.G. 11 (1974) 39-46.

[8]   J. Sehgal, S. Ito, A New Low-Brittleness Glass in the Soda-Lime-Silica Glass Family, J. Am. Ceram. Soc. 81 (1998) 2485-2488.

[9]   B. Lawn, D. Marshall, Hardness, Toughness, and Brittleness: An Indentation Analysis, J. Am. Ceram. Soc. 62 (1979) 347–350.

[10] Y. Kato, H. Yamazaki, S. Yoshida, J. Matsuoka, Effect of densification on crack initiation under Vickers Indentation test, J. Non-Cryst. Solids. 356 (2010) 1768–1773.

[11] T. Rouxel, Driving Force for Indentation Cracking in Glass: Composition, pressure and temperature dependence, Phil. Trans. R. Soc. A. 373 (2015) 20140140.

[12] F. Farges, A Ti K-edge EXAFS Study of the Medium Range Environment around Ti in Oxide Glasses, J. Non-Cryst. Solids. 244 (1999) 25–33.

[13] F. Farges, G.E.J. Brown, A. Navrotsky, H. Gan, J.J. Rehr, Coordination Chemistry of Ti(IV) in Silicate Glasses and Melts: II. Glasses at Ambient Temperature and Pressure, Geochim. Cosmochim. Acta. 60 (1996) 3039–3053.

[14] R. Shannon, Revised Effective Ionic-Radii and Systematic Studies of Interatomic Distances in Halides and Chalcogenides, Acta Crystallogr. Sect. A. 32 (1976) 751–767.

[15] E. Whittake, R. Muntus, Ionic Radii for use in Geochemistry, Geochim. Cosmochim. Acta. 34 (1970) 945-956.

[16] P. Sellappan, T. Rouxel, F. Celarie, E. Becker, P. Houizot, R. Conradt, Composition Dependence of Indentation Deformation and Indentation Cracking in Glass, Acta Mater. 61 (2013) 5949–5965.

[17] M. Guerette, L. Huang, A simple and convenient set-up for high-temperature Brillouin light scattering, J. Phys. D: Appl. Phys. 45 (2012) 275302.

[18] C. Zwikker, Physical Properties of Solids Materials, 2nd ed., Interscience Publishers, New York, 1954.

[19] A. Makishima, J. Mackenzie, Calculation of Bulk Modulus, Shear Modulus and Poisson's Ratio of Glass, J. Non-Cryst. Solids. 17 (1975) 147–157.

[20] S. Inaba, S. Fujino, K. Morinage, Young's Modulus and Compositional Parameters of Oxide Glasses, J. Am. Ceram. Soc. 82 (1999) 3501–507.

[21] G.S. Henderson, M.E. Fleet, The Structure of Titanium Silicate Glasses Investigated by Si K-edge X-ray Absorption Spectroscopy., J. Non-Cryst. Solids. 211 (1997) 214–221.

[22] F. Farges, G.E.J. Brown, J.J. Rehr, Coordination Chemistry of Ti(IV) in Silicate Glasses

and Melts: I. XAFS Study of Titanium Coordination in Oxide Model Compounds, Geochim. Cosmochim. Acta. 60 (1996) 3023–3038.

[23] F. Farges, Coordination of Ti in Crystalline Fresnoites: A High-resolution XANES Spectroscopy Study at the Ti K-edge, J. Non-Cryst. Solids. 204 (1996) 53–64.

[24] Boussinesq J. 1885 *Applications des potentiels aÌ l'étude de l'équilibre et du mouvement des solides élastiques.* Paris, France: Gauthier-Villars.

[25] S. Striepe, J. Deubener, M. Smedskjaer, M. Potuzak, Environmental effects on fatigue of alkaline earth aluminosilicate glass with varying fictive temperature, J. Non-Cryst. Solids. 379 (2013) 161–168.